A Theory of Pitch for the Hydrodynamic Properties of Molecules, Helices, and Achiral

Swimmers at Low Reynolds Number

Anderson D. S. Duraes¹ and J. Daniel Gezelter¹

251 Nieuwland Science Hall,

Department of Chemistry & Biochemistry,

University of Notre Dame, Notre Dame, Indiana 46556, USA

(*Electronic mail: gezelter@nd.edu)

(Dated: 11 September 2023)

Abstract

We present a theory for pitch, a matrix property which is linked to the coupling of rotational

and translational motion of rigid bodies at low Reynolds number. The pitch matrix is a

geometric property of objects in contact with a surrounding fluid, and it can be decomposed

into three principal axes of pitch and their associated moments of pitch. The moments of

pitch predict the translational motion in a direction parallel to each pitch axis when the

object is rotated around that axis, and can be used to explain translational drift, particularly

for rotating helices. We also provide a symmetrized boundary element model for blocks of

the resistance tensor, allowing calculation of the pitch matrix for arbitrary rigid bodies. We

analyze a range of chiral objects, including chiral molecules and helices. Chiral objects

with a C_n symmetry axis with n > 2 show additional symmetries in their pitch matrices.

We also show that some achiral objects have non-vanishing pitch matrices, and use this

result to explain recent observations of achiral microswimmers. We also discuss the small,

but non-zero pitch of Lord Kelvin's isotropic helicoid.

1

I. INTRODUCTION

Screws are simple machines which are universally used to join parts together and to provide secure enclosures for containers. We often draw a distinction between mechanical screws, which move through solid media, and screws which move through a fluid medium, such as self-propelled swimmers. In all cases, the function and efficiency of the screw is associated with the translation-rotation coupling in the medium, which converts rotation around an axis to linear motion along that axis. The translation-rotation coupling is quantified by the screw's pitch, which is the distance the screw translates upon completing one revolution. This is an intuitive approach for screws that involve contact between two solid surfaces. For example, a nut advancing through consecutive threads of a screw travels exactly the distance between threads in a single 2π -radian revolution.

For swimmers and other hydrodynamic screws, where physical threads are not explicit, pitch may be an empirically-measured quantity that is challenging to obtain.² When the screw operates in a fluid, like a propeller operating in seawater, the translation-rotation coupling decreases because of slip along the screw's surface.³ Schamel *et al.*⁴ and Patil *et al.*⁵ observed this fact when studying helical systems moving in liquid media: the translational motion of the helices in a 2π -revolution was less than the standard pitch definition for a helix, which is the distance between consecutive helical turns.

Translational motion can be generated either by rotating the screw itself or induced by rotating the medium around the screw. Howard *et al.* first observed the translational motion of macroscopic chiral objects induced by the vorticity of a fluid.⁶ In their experiment, they suspended dextro-tartaric acid crystals on one side of a drum that was filled with Isopar H (isoparaffinic hydrocarbons). Then, they rotated the drum and observed the migration of the crystals due to the vorticity of the fluid. Although tartaric acid crystals do not look like traditional screws, left- and right-handed crystals exhibit opposite signs of the translational-rotational portion of their resistance tensors, which govern frictional forces and torques experienced by a body in a fluid. This behavior can be used to separate bodies of opposing handedness, since they move in opposite directions in response to rotations. In an earlier paper, we explored the link between parts of the resistance tensor and the translational-rotational coupling, and derived a geometric quantity we called "scalar pitch".⁷ The scalar pitch is a rotational invariant for rigid bodies, describing how the object will translate in response to rotations.

In this paper, we extend the concept of pitch that was developed in Ref. 7 into a matrix form,

and we investigate the physical properties of the characteristic eigenvalues and eigenvectors of this pitch matrix. This results in a method in which chiral (and achiral) objects can be assigned *principal axes of pitch*, and three associated *moments of pitch* for motion around those axes. In previous work, the method used for computing resistance tensors was aimed at studying pitch in molecules, so spherical beads representing the atoms were the primary hydrodynamic elements. In this paper, we develop a symmetrized boundary element method using triangular surface patches to evaluate resistance tensors for arbitrary shapes.

II. FORMALISM

A. Resistance and Mobility Tensors

Consider an arbitrarily shaped rigid body moving in a fluid at low Reynolds number. This rigid body will feel a force and torque in response to its velocity and angular velocity in the fluid. For example, a propeller placed in a flowing fluid experiences a torque, while a screw rotating through a quiescent medium experiences a linear force.

We define a coordinate system whose origin, O, is moving with the body. From Brenner's fundamental work on hydrodynamics, ^{8,9} the relationship among net force (\mathbf{f}), torque ($\boldsymbol{\tau}$), velocity (\mathbf{v}) and angular velocity ($\boldsymbol{\omega}$) at O is:

$$\begin{bmatrix} \mathbf{f} \\ \boldsymbol{\tau} \end{bmatrix} = -\Xi \begin{bmatrix} \mathbf{v} \\ \boldsymbol{\omega} \end{bmatrix}, \text{ where } \Xi = \begin{bmatrix} \Xi^{\text{tt}} & \Xi_O^{\text{rt}} \\ \Xi_O^{\text{tr}} & \Xi_O^{\text{rr}} \end{bmatrix}. \tag{1}$$

 Ξ is a 6×6 hydrodynamic resistance tensor that provides details on how the body couples to the surrounding medium. The four blocks of Ξ represent the translational (tt), rotational (rr), translation-rotation (tr) and rotation-translation (rt) coupling of the body to the medium. The (rt) coupling is the matrix transpose of the (tr) coupling, $\Xi_O^{\rm rt} = \left(\Xi_O^{\rm tr}\right)^T$, and the subscript O indicates the quantities which depend on the location of the reference point O.

The inverse of the resistance tensor is known as the mobility tensor, ¹⁰

$$\boldsymbol{\mu} = \begin{bmatrix} \mu_O^{\text{tt}} & \mu_O^{\text{rt}} \\ \mu_O^{\text{tr}} & \mu^{\text{rr}} \end{bmatrix} = \Xi^{-1} \,. \tag{2}$$

 μ also comprises four blocks that are analogous to the blocks of the hydrodynamic resistance tensor Ξ defined in Eq. (1). Multiplying the mobility tensor by k_BT yields the diffusion tensor, which is a generalization^{9,10} of Einstein's relation,¹¹ connecting the resistance and diffusion tensors.

B. The Pitch Matrix

Imagine a simple screw advancing through a material. Because it is coupled to the surrounding medium, if the screw rotates by an angle ϕ around its long axis (z), it moves linearly along the same rotation axis,

$$\Delta z = \frac{P}{2\pi} \Delta \phi. \tag{3}$$

This defines the pitch P of the screw in terms of a full 2π rotation in ϕ .

For continuous rotation in a medium, we can similarly define the pitch in terms of linear and angular velocities of the screw as it rotates around a single axis (z),

$$v_z = \frac{P}{2\pi} \,\omega_z \tag{4}$$

More generally, the screw may be moving with a (space-fixed) angular velocity vector (ω) and the resultant motion may also be a linear velocity vector (\mathbf{v}). In this case, the relationship between ω and \mathbf{v} is mediated by a 3×3 pitch matrix,

$$\mathbf{v} = \frac{\mathsf{P}}{2\pi} \,\omega \tag{5}$$

Modeling a rigid body as a power screw (which is driven solely by an imposed torque) implies a net force $\mathbf{f} = 0$ in Eq. (1). ^{12,13} We can then equate the drag force from translational motion to the rotational contribution of the force on the object,

$$\Xi^{\text{tt}} \mathbf{v} = -\Xi_O^{\text{rt}} \boldsymbol{\omega} \tag{6}$$

We can then use the definition of the pitch matrix in Eq. (5), and obtain an expression in terms of two blocks of the resistance tensor,

$$\Xi^{\text{tt}} \mathbf{v} = \Xi^{\text{tt}} \frac{\mathsf{P}_O}{2\pi} \boldsymbol{\omega} = -\Xi_O^{\text{rt}} \boldsymbol{\omega} \tag{7}$$

which implies

$$\frac{\mathsf{P}_O}{2\pi} = -\left(\Xi^{\mathsf{tt}}\right)^{-1} \, \Xi_O^{\mathsf{rt}} \tag{8}$$

where $\frac{P_O}{2\pi}$ can be seen as a quantity that also depends on the point O.

It is also possible to write an equivalent expression for the pitch matrix in Eq. (8) using two blocks of the mobility tensor. From Eq. (2), the relation between the resistance and mobility tensors can be rewritten as

$$\Xi \mu = \begin{bmatrix} \mathbf{I} & \mathbf{0} \\ \mathbf{0} & \mathbf{I} \end{bmatrix}, \tag{9}$$

where **I** is the 3×3 identity matrix and **0** is the 3×3 null matrix. In terms of the mobility tensor blocks, the pitch matrix is:

$$\frac{\mathsf{P}_O}{2\pi} = \mu_O^{\mathsf{rt}} \left(\mu^{\mathsf{rr}}\right)^{-1} \tag{10}$$

Note that Eqs. (8) and (10) are equivalent forms.

We note that when a rigid body is settling under an external force, so that translational motion generates all rotation, we must invoke a different process than a power screw, as the force on the body is no longer zero. In this case, we have no external torque ($\tau = 0$) and $\omega = Lv$, where L is a 3×3 matrix that mediates the generation of angular velocity from linear velocity. Using the resistance or mobility tensors,

$$L = -\left(\Xi_O^{\rm rr}\right)^{-1} \Xi_O^{\rm tr} = \mu_O^{\rm tr} \left(\mu_O^{\rm tt}\right)^{-1} , \qquad (11)$$

which can be related to the pitch matrix defined in Eqs. (8) or (10),

$$\frac{\mathsf{P}_O}{2\pi} = \left(\Xi^{\mathsf{tt}}\right)^{-1} \mathsf{L}^T \left(\Xi_O^{\mathsf{rr}}\right) = \mu_O^{\mathsf{tt}} \mathsf{L}^T \left(\mu^{\mathsf{rr}}\right)^{-1}. \tag{12}$$

Ekiel-Jeżewska and Wajnryb¹⁴ studied this process using a three-sphere (trumbbell) model settling under gravity in a viscous fluid and concluded that the trumbbell rotates as it settles. In Sec. III C, we consider a similar example using an isotropic helicoid falling through a fluid, where its linear velocity induces a small angular velocity.

C. Center of Pitch

The translational (tt) and rotational (rr) blocks of the resistance (Eq. (1)) and mobility (Eq. (2)) tensors are symmetric matrices for any point O. However, the blocks which couple translation and rotation are only symmetric at the center of resistance (CR) for the resistance tensor,^{7–9} and at the center of diffusion (CD) for the mobility tensor.^{7,9} Therefore, the pitch matrix is not generally a symmetric matrix. However, at one special point, which we call the *center of pitch* (\mathbf{p}), the pitch matrix does become symmetric.

For the resistance tensor, the translation-rotation couplings at a point M (separate from the origin) will include a portion of the translational block along the line connecting the origin O to M, while the translation-rotation couplings for the mobility tensor will include a portion of the rotational block.^{7–9} We can express the new couplings,

$$\Xi_M^{\text{tr}} = \Xi_O^{\text{tr}} - \mathsf{U}_M \Xi^{\text{tt}} \tag{13}$$

$$\mu_M^{\text{tr}} = \mu_O^{\text{tr}} + \mu^{\text{rr}} \mathsf{U}_M \tag{14}$$

where U_M is a skew-symmetric matrix whose elements are set by the vector from point O to point M,

$$U_{M} = \begin{bmatrix} 0 & -z_{OM} & y_{OM} \\ z_{OM} & 0 & -x_{OM} \\ -y_{OM} & x_{OM} & 0 \end{bmatrix}.$$
 (15)

Note that $(\mathsf{U}_M)^T = -\mathsf{U}_M$.

Left-multiplying the transpose of Eq. (13) by $(\Xi^{tt})^{-1}$, or right-multiplying the transpose of Eq. (14) by $(\mu^{rr})^{-1}$, we can see how to transform a pitch matrix computed at a point O to another point M,

$$\frac{\mathsf{P}_M}{2\pi} = \frac{\mathsf{P}_O}{2\pi} - \mathsf{U}_M \tag{16}$$

To find the center of pitch, or the point \mathbf{p} where the pitch matrix is symmetric, we set the right side of Eq. (16) equal to its transpose and we find the coordinates of the vector $\mathbf{r}_{\mathbf{p}}$ connecting the center O to \mathbf{p} :

$$\mathbf{r_p} = \frac{1}{4\pi} \begin{bmatrix} (P_O)_{zy} - (P_O)_{yz} \\ (P_O)_{xz} - (P_O)_{zx} \\ (P_O)_{yx} - (P_O)_{xy} \end{bmatrix}$$

where the subscripts indicate the entries of the P_O matrix. The supplementary material (Sec. I) provides an additional proof that the center of pitch is unique to each body.

The symmetric pitch matrix can be found without knowing the center of pitch,

$$\mathsf{P}_{\mathbf{p}} = \frac{1}{2} \left[\mathsf{P}_O + \mathsf{P}_O^T \right]. \tag{17}$$

However, this relation does not provide the location of the center of pitch.

D. Pitch Axes, Moments of Pitch, and The Pitch Coefficient

From the original definition of pitch (Eq. (5)), we can diagonalize ¹⁵ the symmetric pitch matrix and write

$$A^{-1} \left(\frac{P_{\mathbf{p}}}{2\pi} \right) A = \begin{bmatrix} \lambda_1 & 0 & 0 \\ 0 & \lambda_2 & 0 \\ 0 & 0 & \lambda_3 \end{bmatrix}$$
 (18)

where the three eigenvalues (λ_i) are moments of pitch — each associated with a pitch axis, α_i — which is one of the column vectors making up $A = [\alpha_1, \alpha_2, \alpha_3]$. This decomposition into principal

axes and moments of pitch is a direct analogy to the decomposition of a moment of inertia tensor into principal axes and moments of inertia. For the pitch matrix, however, moments of pitch may be negative if rotating the body counterclockwise around axis α_i results in translation along the negative α_i direction.

It is useful to define a rotational invariant which will provide information on the average translational motion exhibited when the body has a random orientation in the fluid. We can define a *scalar pitch coefficient* which is the simplest rotational invariant of the pitch matrix, providing

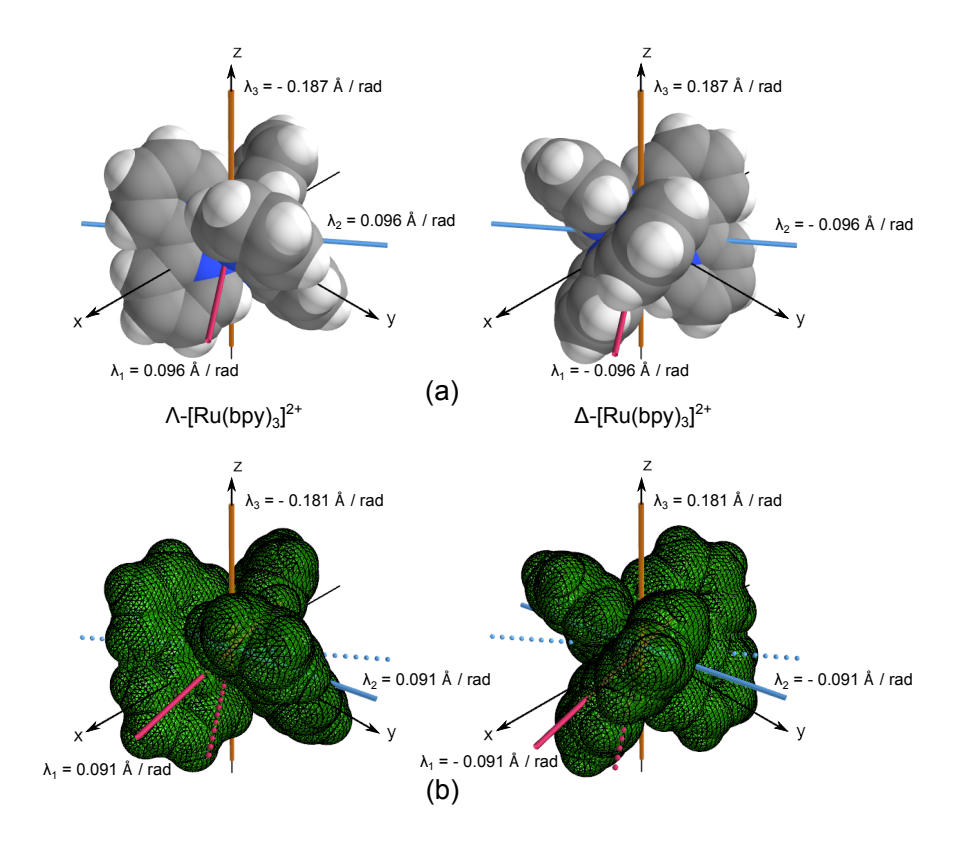


FIG. 1. The pitch axes and the moments of pitch for the Λ and Δ enantiomers of the $[Ru(bpy)_3]^{2+}$ ion. In the upper panel (a), spheres with radii from the OPLS-AA force field were used to compute the resistance tensor, while in the lower panel (b), a triangulated surface mesh was utilized. The two enantiomers have opposing signs for all three of their moments of pitch. Note that two moments of pitch are degenerate, indicating that a linear combination of the corresponding pitch axes will also form a basis along the xy-plane (the pink and blue lines or the pair of dotted lines in the lower panel, for example). The pitch axis along the z-axis is aligned with the C_3 axis of the molecule. The scalar pitch coefficient for this molecule is $|P|/2\pi = 0.133 \text{ Å/rad}$.

equal contributions from rotation around all three axes of pitch,

$$\frac{|P|}{2\pi} = \sqrt{\frac{1}{3} \sum_{i} \lambda_i^2} \tag{19}$$

The derivation of the *scalar pitch coefficient* is available in Sec. II of the supplementary material. Note that this is functionally equivalent to a pitch coefficient that was demonstrated in our previous paper,⁷ where the eigenvalues of the (tt) and (tr) blocks were used separately to compute $|P|/2\pi$.

Figure 1 displays the principal axes of pitch and their associated moments for the Λ and Δ enantiomers of the $[Ru(bpy)_3]^{2+}$ ion. If there are degeneracies in the moments of pitch, a linear combination of the corresponding pitch axes will also form a basis for understanding the translation-rotation coupling of the object.

E. Pitch Properties of Enantiomers and Achiral Objects

Consider a left- and right-handed pair of enantiomers, whose structures are related by a reflection through the origin. For enantiomers, the (tt) and (rr) blocks of the resistance and mobility tensors will be identical, while the (tr) and (rt) blocks flip sign. Using this mirror image property, we can deduce the following property of the pitch matrix for the two enantiomers:

$$\left(\frac{\mathsf{P}_O}{2\pi}\right)^{\text{left}} = -\left(\frac{\mathsf{P}_O}{2\pi}\right)^{\text{right}} \tag{20}$$

At the center of pitch, Eq. (20) implies that the moments of pitch (eigenvalues) of the pitch matrix for the left- and right-handed objects have the same magnitude, but flip signs. The pitch axes (eigenvectors), however, are identical for both objects.

For an achiral object, which is identical with its own mirror image, the characteristic eigenvalues of the left and right pitch matrices must be the same, and there are two ways for this to happen:

1)
$$\lambda_1 = \lambda_2 = \lambda_3 = 0$$

In this case, the achiral object has a pitch matrix which is the null matrix, and thus does not exhibit displacement due to rotation. This situation occurs in objects with a high degree of internal symmetry, *e.g.*, spheres and ellipsoids.

2) $\lambda_1 = 0$ and $\lambda_2 = -\lambda_3 \neq 0$ In this case, the achiral object has a pitch matrix which is non-zero. These objects can exhibit displacement due to rotation, and this property helps explain the recent observation of achiral microswimmers which can be propelled through a fluid via rotation¹⁷ (see Fig. 2).

For chiral objects, there are two additional cases to consider:

- 3) $\lambda_1 = \lambda_2 \neq \lambda_3$ (two degenerate eigenvalues). This class of objects is a chiral body in the C_n or D_n point groups with $n \geq 3$.
- 4) $\lambda_1 \neq \lambda_2 \neq \lambda_3$ This is the general case for most chiral objects without higher symmetry axes.

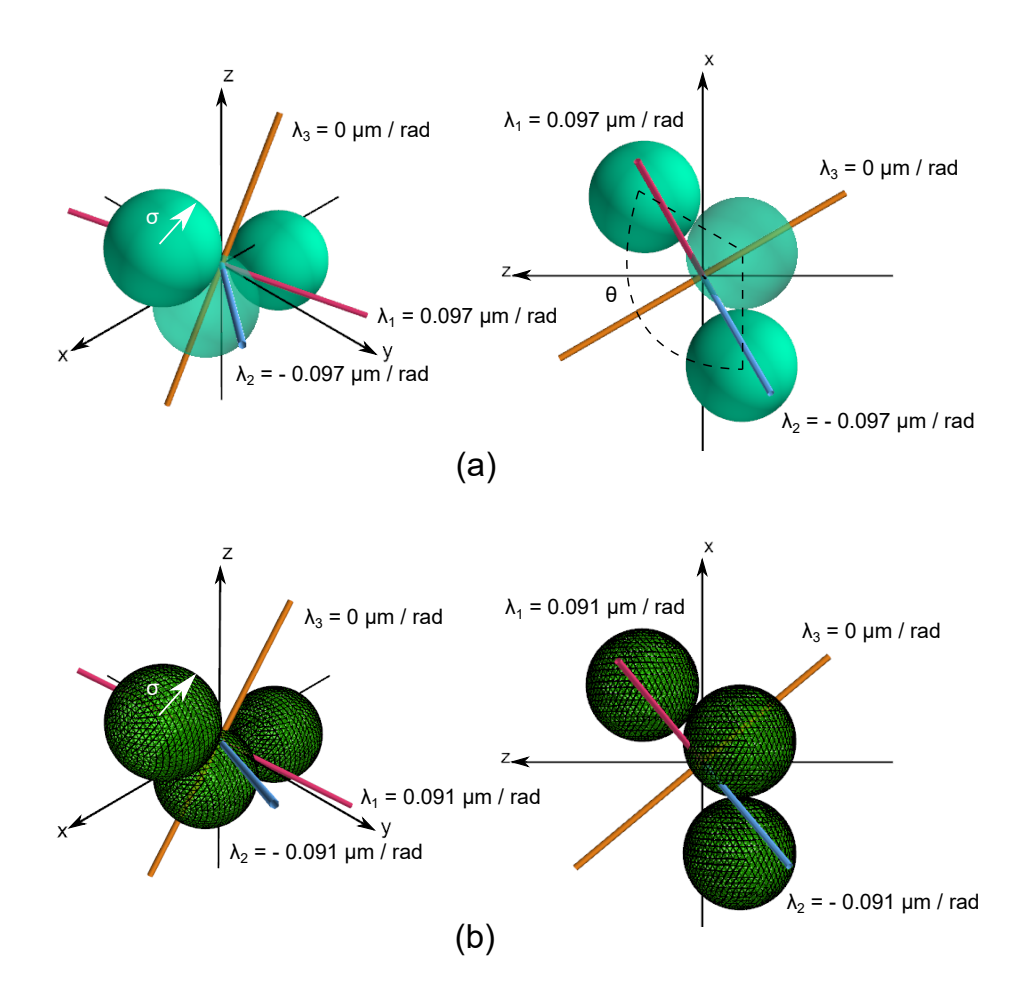


FIG. 2. Achiral swimmers, like the three bead arrangement shown here, can exhibit non-zero pitch matrices and two moments of pitch with opposite signs. This means that rotation of these swimmers can result in translation through a fluid. In this collection of particles, each of the three beads has a radius of $\sigma = 2.2 \,\mu\text{m}$ and an angle $\theta = 120^{\circ}$. This corresponds to class 2 in the classification of achiral objects. In the upper panel (a), spheres were used to compute the resistance tensor, while in the lower panel (b), a triangulated surface mesh was utilized.

To explore the pitch matrix properties of chiral objects, we can consider the chiral point groups C_n and D_n .¹⁸ Table I shows the moments of pitch (the eigenvalues of the pitch matrix) for a set of representative molecules that belong to the C_n and D_n point groups.^{19–21} To compute these moments of pitch, we first constructed the molecular resistance tensors, representing atoms with spheres with appropriate van der Waals radii. The molecular resistance tensors were computed using the methods described in Ref. 7. The pitch matrix for each molecule was then constructed and diagonalized to obtain the molecular pitch axes (eigenvectors) and the associated moments of pitch (eigenvalues).

When the symmetry axis of the point groups has $n \ge 3$, we find that two of the moments of pitch are always degenerate (see table I). When this degeneracy occurs, the *non*-degenerate moment of pitch is associated with a pitch axis that points directly along the C_n axis of the molecule. This property is expected from the character tables of the C_n and D_n point groups,²² since one coordinate (e.g., z) forms a basis for a *non*-degenerate irreducible representation, and the other two coordinates (e.g., x) and y span a doubly-degenerate representation.

TABLE I: Moments of Pitch for representative molecules from the chiral point groups C_n and D_n . ^{19–21} To compute molecular resistance tensors, atoms were represented with spheres with appropriate van der Waals radii, and resistance tensors were computed using the methods described in Ref. 7. Degenerate moments of pitch are indicated in bold type.

Daint Cross	Malagula	Moments of Pitch ($\times 10^{-4} \text{ Å rad}^{-1}$)		
Point Group	Molecule	λ_1	λ_2	λ_3
	1-bromo-1-chloroethane	-229.32	11.07	223.36
	2,3-dihydrofuran	-210.45	-17.25	240.34
	bromochlorofluoromethane	-156.89	22.91	134.06
C_1	D-alanine	-404.01	60.99	375.02
	D-serine	-384.40	2.37	338.14
	SOClBr	-119.43	-14.30	133.58
	1,3-dichloroallene	-477.66	-25.93	583.70
	2,3-pentadiene	-250.60	-182.19	405.21
	cis-[Co(en) ₂ Cl ₂] ⁺	-306.88	91.10	145.42
C_2	hydrazine	-324.38	-16.05	256.58
	hydrogen peroxide	-273.39	-199.04	408.42
	Mo(acac) ₂ O ₂	-1323.32	4.85	1266.70
	titanium dimer	-366.93	-212.78	600.78
Continued on next page				n next page

TABLE I – continued from previous page

Daint Consu	M.L.	Moments of Pitch ($\times 10^{-4} \text{ Å rad}^{-1}$)		
Point Group	Molecule	λ_1	λ_2	λ_3
	tris-aminomethane	-119.09	-119.09	178.09
	triethylamine	-110.35	36.66	36.66
C_3	triphenylmethane	-1071.89	-1071.89	2056.39
	triphenylphosphine	-857.58	-857.58	1645.00
C_4	tetra-aza copper(II)	-85.70	-85.70	110.43
C_5	C_5 Fe(Me ₅ -Cp)(P ₅)		11.47	11.47
C_6	C ₆ alpha-cyclodextrin		-9.79	34.49
	biphenyl	-1730.16	605.84	1144.82
D_2	trans-[Co(en) ₂ Cl ₂] ⁺	-153.73	79.32	90.63
	twistane	-92.72	20.74	40.50
	guanidinium cation	-39.67	81.99	81.99
D_3	tris(en)cobalt(III)	-176.32	-176.32	328.17
	tris(oxalato)iron(III)	-402.24	-402.24	953.13
D_4	tetrathiacyclododecane	-218.66	325.53	325.53
D	twisted ferrocene	-14.26	10.73	10.73
D_5	YbI ₂ (THF) ₅	-180.88	-180.88	356.50
D_6	bis(benzene)chromium	-4.43	3.51	3.51

F. Hydrodynamic Model: Determining the Resistance Tensor from Triangulated Surfaces

The exterior surface of any rigid body moving through a fluid can be described as a surface mesh comprising small, flat triangular patches. Surface triangulation is a widely-researched topic, and we assume here that the object of interest has been expressed in this form. When viscous forces are dominant, *i.e.*, at low Reynolds number, the velocity of triangle i (\mathbf{v}_i) is related to the unperturbed velocity of the fluid (\mathbf{u}) via hydrodynamic interaction tensors (\mathbf{B}_{ij}), which connect triangular plate i to the forces experienced by all of the triangular plates comprising the surface of the rigid body,²³

$$\mathbf{v}_i = \mathbf{u} - \sum_j \mathsf{B}_{ij} \mathbf{F}_j \tag{21}$$

Because the hydrodynamic interaction is reciprocal,²⁴ we introduce a symmetrized version of B which integrates over both triangular patches to obtain coupling between triangular elements,

$$\mathsf{B}_{ij} = \mathsf{B}_{ji} = \frac{1}{2} \left[\frac{1}{A_j} \int_{S_j} \mathsf{T}(\mathbf{x}_i, \mathbf{y}) \, d\mathbf{y} + \frac{1}{A_i} \int_{S_i} \mathsf{T}(\mathbf{x}_j, \mathbf{y}) \, d\mathbf{y} \right]$$
(22)

These are integrals over the surfaces S_j and S_i of triangles j and i, respectively, and \mathbf{x}_i is the centroid (or barycenter) of triangle i. The area of triangle j can be similarly expressed as a surface integral,

$$A_j = \int_{S_j} d\mathbf{y} \ . \tag{23}$$

The symmetrized form of B is essential for maintaining the known properties of the resistance tensor (Sec. II C).

The Oseen tensor connecting points **a** and **b**, 23,24

$$T(\mathbf{a}, \mathbf{b}) = T(\mathbf{b}, \mathbf{a}) = \frac{1}{8\pi \eta |\mathbf{a} - \mathbf{b}|} \left[\mathbf{I} + \frac{(\mathbf{a} - \mathbf{b}) \otimes (\mathbf{a} - \mathbf{b})}{|\mathbf{a} - \mathbf{b}|^2} \right]$$
(24)

provides the coupling through a surrounding fluid with dynamic viscosity η . The \otimes symbol indicates the outer (tensor) product of two vectors, in this case, $(\mathbf{a} - \mathbf{b})$ with itself.

The surface integrals in Eq. (22) can be calculated numerically using a surface quadrature:

$$\frac{1}{A_{j}} \int_{S_{j}} \mathsf{T}(\mathbf{x}_{i}, \mathbf{y}) d\mathbf{y} \approx \frac{1}{A_{j}} \left[A_{j} \sum_{k} w_{k} \mathsf{T}(\mathbf{x}_{i}, \mathbf{y}_{k_{j}}) \right]$$

$$\approx \sum_{k} w_{k} \mathsf{T}(\mathbf{x}_{i}, \mathbf{y}_{k_{j}}), \tag{25}$$

where w_k is a weight associated with the quadrature point \mathbf{y}_{k_j} on triangle j, and \mathbf{x}_i is the centroid of triangle i. Using quadrature points and weights, we can therefore rewrite Eq. (22) as:

$$\mathsf{B}_{ij} = \frac{1}{2} \sum_{k} w_k \left[\mathsf{T}(\mathbf{x}_i, \mathbf{y}_{k_j}) + \mathsf{T}(\mathbf{x}_j, \mathbf{y}_{k_i}) \right]$$
 (26)

If not stated otherwise, we employ a 6-point Gaussian quadrature developed by Cowper²⁵ which exactly integrates polynomials of degree 3 and whose points and weights are available in Quadpy.²⁶ Because the centroid is not a point in this quadrature, there is no singularity in the self interaction (B_{ii}).

Using all of the 3×3 B_{ij} matrices, we can construct a $3N \times 3N$ B supermatrix, where N stands for the total number of triangular plates, and rewrite Eq. (21) as,

$$\mathbf{V} - \mathbf{U} = -\mathbf{B}\mathbf{F}.\tag{27}$$

where V, U, and F are 3N-dimensional vectors representing the triangles' velocities, unperturbed fluid velocity, and forces on all of the triangles. The solution of Eq. (27) to find the force requires the inverse, $C = B^{-1}$,

$$\mathbf{F} = -\mathbf{C}(\mathbf{V} - \mathbf{U}),\tag{28}$$

and is equivalent to the translational block of the resistance tensor in Eq. (1), after summing over all the triangles to yield the net translational force on the object,

$$\mathbf{f} = -\left(\sum_{ij} C_{ij}\right) \mathbf{v}$$
$$= -\Xi^{tt} \mathbf{v}$$

where C_{ij} are the 3×3 blocks of the C matrix, and we have assumed that the assembly of triangles is a rigid body, so all triangles have the same velocity relative to the fluid, $(\mathbf{v}_j - \mathbf{u}) = \mathbf{v}$. This allows us to identify the translational resistance tensor, $^{27-29}$

$$\Xi^{tt} = \sum_{ij} \mathsf{C}_{ij} \tag{29}$$

From the Brenner relations for the (tr) and (rr) blocks of the resistance tensor in a discrete, matrix form, ^{7–9} we also have

$$\Xi_O^{\text{tr}} = \sum_{ij} \mathsf{U}_i \mathsf{C}_{ij},$$

$$\Xi_O^{\text{rr}} = -\sum_{ij} \mathsf{U}_i \mathsf{C}_{ij} \mathsf{U}_j$$
(30)

where U_i is the skew-symmetric matrix defined in Eq. (15) whose entries x_{Oi} , y_{Oi} and z_{Oi} are the components of the vector between the origin O and the centroid of the triangle i.

Note that in contrast to bead models,^{7,28–30} a boundary element method does not require a volume correction to the rotational block of the resistance tensor, since the boundary element method computes interactions using hydrodynamic elements that have no volume.

With the blocks of the resistance tensor computed at point O, it is possible to reconstruct the blocks at another point M. The (tt) block is invariant to choice of origins, the (tr) block follows Eq. (13), and the (rr) block requires coupling to the other blocks of Ξ , $^{7-9}$

$$\Xi_M^{\rm rr} = \Xi_O^{\rm rr} + \Xi_O^{\rm tr} \mathsf{U}_M - \mathsf{U}_M \left(\Xi_O^{\rm tr}\right)^T - \mathsf{U}_M \Xi^{\rm tt} \mathsf{U}_M \tag{31}$$

In Sec. III of the supplementary material, we apply the boundary element method developed here to objects whose blocks of the resistance tensor are known analytically. The boundary element method shows good agreement with the analytical values.

III. RESULTS

Applying the triangulated surface boundary element method described in the previous section, we have computed the principal axes of pitch and moments of pitch for a wide array of objects. These objects include common chiral entities like helices, achiral swimmers, and one object of historical curiosity: Lord Kelvin's Isotropic Helicoid. These objects are swimming at low Reynolds number and, if not stated otherwise, we shifted the center of pitch to the origin of the coordinate system. Wherever possible, we compare the predictions from the pitch matrix to experimental results for similar objects in similar fluid conditions. For Lord Kelvin's Isotropic Helicoid, we also investigate two feasible experiments to assess its rotation-translation coupling.

A. Chiral Objects

1. Helices

The hydrodynamic properties of helices have been studied widely because of their importance in the motion of living cells. Chwang and Wu³¹ and Higdon³² used a helix connected to a spherical head to model the swimming of microorganisms and to find optimum design parameters for efficient propulsion under low Reynolds numbers. Purcell³³ approximated the blocks of the resistance tensor in Eq. (1) as scalars, reducing the 6×6 resistance tensor to a 2×2 tensor, and explored the relation between these scalar values in the coupling of translational and rotational motions of helical systems. To study the swimming properties of *Escherichia coli* bacteria, Chattopadhyay *et al.*³⁴ utilized the same scalar approach as Purcell and estimated the reduced 2×2 resistance tensor using optical tweezers to trap a sample of swimming *E. coli*. Recently, Maffeo *et al.*³⁵ have looked at using rotating nucleic acid double helices as turbines, using electric fields to drive the motion of these molecules.

The work on helical molecules is at a length scale where the theory of pitch may help guide design parameters for molecular machines. To test these ideas, it is important to determine if the pitch matrix can reproduce previous work on helical systems in general. In this section, we first discuss the pitch matrix properties of a single microhelix using the hydrodynamic model developed in Sec. II F to compute the 6×6 resistance tensor. In the following section, we apply this work to three primary structures of DNA double helices.

To test the pitch matrix properties for a simple helix, we constructed a 3 μ m right-handed helix

with an outside diameter of 0.5 μ m and a thickness of 0.2 μ m using spherical beads. The helix was constructed through a procedure outlined in the Supporting Information of Ref. 7, where the centers of consecutive beads are 0.049 μ m apart. To triangulate the surface mesh (see Fig. 3) and compute the resistance tensor and pitch matrix for the helix, we used the MSMS algorithm³⁶ with a probe radius large enough (0.2 μ m) to smooth the helical surface. Figure 3 presents the principal axes of pitch and the associated moments of pitch for motion around these axes. None of the principal axes of pitch lie along the long axis (z-axis) of the helix. Therefore, a rotation around the helical z-axis will result in translational drift, whose direction is indicated by the vector \mathbf{v} in Fig. 3(b).

Using the pitch matrix computed at the center of pitch, we can predict the resulting motion for this helix as it rotates around the z-axis. With an angular velocity $\omega = (0,0,1)$ rad s⁻¹ and using Eq. (5), the resulting translational velocity for this helix is $\mathbf{v} = (0.00970, 0.0120, 0.0242) \,\mu\text{m s}^{-1}$. The translational motion of the helix will be along the vector \mathbf{v} , and the projected distance of travel,

$$d = |\mathbf{v}| \times t = \frac{|\mathbf{v}|}{|\omega|} \times |\omega| t \tag{32}$$

where t is the total time.

From Chasles' theorem,³⁷ which states that rigid body motion can be decomposed into rotation along an axis and translation parallel to that axis (a screw displacement), the term $|\mathbf{v}|/|\omega|$ in Eq. (32) may be interpreted as the pitch projected along the vector \mathbf{v} . For the helix in Fig. 3, $|\mathbf{v}|/|\omega| = 0.0287 \,\mu\text{m} \,\text{rad}^{-1}$, and thus it will travel a distance $d = 180 \,\text{nm}$ after one complete revolution around the *z*-axis. Because the helix is moving through a fluid, rather than a solid, the distance d is smaller than the designed pitch of the helix, which is 1 μ m per turn. (As in physical screws, the designed pitch of a helix will only be equivalent to the travel from one rotation when the helix is advancing through a solid substrate.)

The constructed helix in Fig. 3 is similar to the microhelices propelled with a magnetic field by Patil *et al.*⁵ We note that this group observed the microhelices drifting and estimated an experimental projected pitch of 250 nm. In Sec. IV of the supplementary material, we also provide data on three helices which approximate those in the Patil *et al.* experiments⁵ and find projected pitch values from 138–280 nm.

To make a direct comparison to experiments, we can use the scalar pitch coefficient, a rotational invariant defined in Eq. (19), which includes contributions from all three pitch axes. In the helix in Fig. 3, the scalar pitch coefficient is calculated to be 125 nm. For helices with flagellar widths

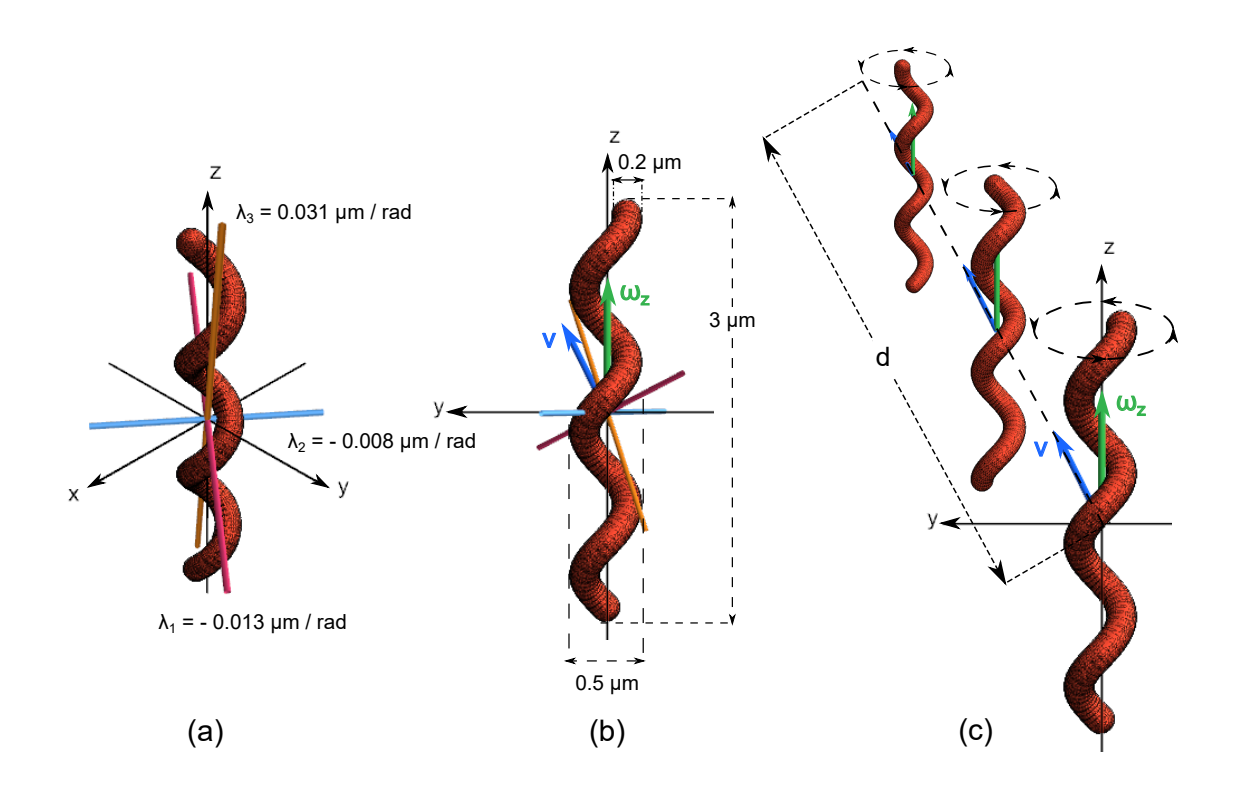


FIG. 3. Pitch of a Right-handed Helix: (a) The principal axes of pitch (pink, blue and orange lines) and the three associated moments of pitch for motion around those axes. (b) Design parameters and the velocity vector \mathbf{v} due to rotation around the z-axis with an angular velocity ω_z . (c) The distance d traveled by this helix after rotating around the z-axis. This distance can be computed by Eq. (32).

ranging from 0.1–0.25 μ m, we find scalar pitch coefficients from 95.5–194 μ m. We also note that the scalar pitch coefficients are all ~70% of the largest of the three moments of pitch, so we can infer that the helix tends to align to the axis of pitch associated with the largest of the three moments. Drifting was also observed by Ceylan *et al.*³⁸ in their experiments with helical microswimmers.

2. Double Helices: A-, B-, and Z-DNA

To study a biologically relevant set of helices, we analyzed molecular structures representing the A, B, and Z forms of DNA. The A-DNA sample is a dodecamer with 3 consecutive CpG steps (PDB code 5MVK),³⁹ the B-DNA sample is a Dickerson-Drew dodecamer (PDB code 4C64),⁴⁰ and the Z-DNA sample is also a dodecamer (PDB code 4OCB).⁴¹ These three DNA structures are all derived from experimental crystal structures.

To triangulate the surface of the DNA samples, we represented the atoms as spheres with appro-

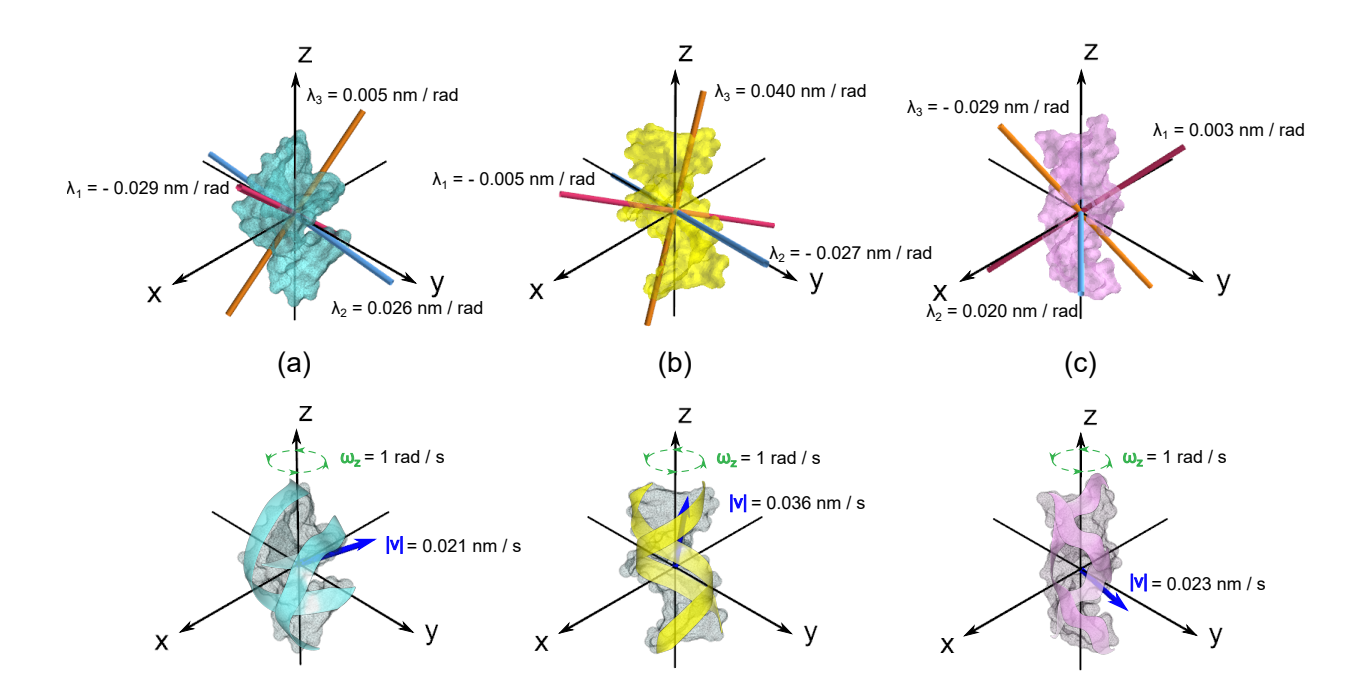


FIG. 4. The three DNA samples: (panel a) A-DNA, (panel b) B-DNA and (panel c) Z-DNA. The principal axes of pitch and their moments of pitch are in the upper panels. The ribbon diagram and the resulting velocity vector caused by a rotation around the *z*-axis are in the lower panels. The ribbon diagram denotes the sugar-phosphate backbones (helices) of the DNA and were generated using the CCP4mg.⁴⁴

priate van der Waals radii and used the MSMS algorithm³⁶ with a probe radius of 1.41 Å to mimic the surrounding water molecules.⁴² We computed the resistance tensor employing the triangulated surface method described in Sec. II F.

In Fig. 4, the upper panels display the pitch axes along with the associated moments of pitch for the three DNA samples and the lower panels, the resulting translational velocity due to a rotation around the z-axis ($\omega_z = 1 \text{ rad s}^{-1}$). The three DNA samples manifest translational drift coupled to the rotation around the z-axis. From Eq. (32), we can compute the pitches projected along the vector \mathbf{v} displayed in the lower panels, $\frac{|\mathbf{v}|}{|\omega|} \times 2\pi = 0.13$ nm (A-DNA), 0.23 nm (B-DNA) and 0.14 nm (Z-DNA). These values are smaller than the average structural pitch (per turn) associated with DNA which are: 2.82 nm (A-DNA), 3.38 nm (B-DNA), and 4.50 nm (Z-DNA). Because the DNA samples are moving in a fluid (and not through a solid substrate), we expect the moments of pitch to be significantly smaller than the structural pitch, since the fluid slips along the surface of the DNA molecules.

In a stationary liquid, using the Einstein relation between mean square displacement and the

TABLE II. Translational diffusion coefficients D_{tt} and scalar pitch coefficients $|P|/2\pi$ (Eq. (19)) for dodecamers of the three helical forms of DNA. The translational diffusion coefficients are based on dilute water solutions at 298.15 K with a viscosity of 0.89 mPa·s. ⁴⁵ Conditions when translation-rotation coupling overtakes translational diffusion are also provided (Eq. (34)).

Structure (PDB code)	$D_{\rm tt} \left(10^8 \ {\rm nm}^2 \ {\rm s}^{-1} \right)$	$ P /2\pi \left(\text{nm rad}^{-1}\right)$	$ \omega ^2 \times t \left(10^{12} \text{ rad}^2 \text{ s}^{-1}\right)$
A-DNA (5MVK)	1.70	0.023	> 1.9
B-DNA (4C64)	1.65	0.028	> 1.3
Z-DNA (4OCB)	1.66	0.020	> 2.5

translational diffusion coefficient $D_{\rm tt}$, 11

$$\langle (\delta r(t))^2 \rangle = 6 D_{tt} t, \qquad (33)$$

we can estimate when the translation-rotation coupling will overcome diffusion. This will happen when the ratio of the distance squared in Eq. (32) to the mean square displacement in Eq. (33) is greater than 1,

$$|\omega|^2 t > 6D_{tt} \left(\frac{|P|}{2\pi}\right)^{-2} \tag{34}$$

where we substituted the term $|\mathbf{v}|/|\omega|$ in Eq. (32) for the scalar pitch coefficient $|P|/2\pi$ in Eq. (19). The diffusion coefficient is calculated as $D_{\rm tt} = \frac{1}{3} {\rm Tr} \; D_{\rm CD}^{\rm tt}, ^{9,29}$ where the matrix $D_{\rm CD}^{\rm tt} = (k_B T) \mu_{\rm CD}^{\rm tt}$ is defined in Eq. (2) and CD stands for the center of diffusion (see Sec. II C). The term $|\omega|^2 t$ is a threshold value which can aid in the design of propulsion experiments.

Table II shows the diffusion coefficients for the DNA samples and the angular velocity conditions for when the translation-rotation coupling overcomes translational diffusion. The translational diffusion coefficients are computed in dilute water solutions at 298.15 K and $\eta = 0.89$ mPa·s. From the angular velocity conditions in Table II, a 11.6-day experiment requires angular velocities, $|\omega|$, that exceed 1.4×10^3 rad s⁻¹ (A-DNA), 1.1×10^3 rad s⁻¹ (B-DNA), and 1.6×10^3 rad s⁻¹ (Z-DNA) to overcome translational diffusion. In longer experiments, as long as rotations are continuous, translation-rotation coupling can overcome diffusion with smaller angular velocities.

In comparison with the DNA samples in Table II, the 3 μ m single helix in Sec. III A 1 has $D_{\rm tt} = 4.39 \times 10^5 \ {\rm nm}^2 \ {\rm s}^{-1}$ when suspended in the same dilute water conditions, with a pitch coefficient of $|P|/2\pi = 19.9 \ {\rm nm} \ {\rm rad}^{-1}$. The $|\omega|^2 t$ threshold value points to the minimum frequency of rotation $|\omega|$ that the helix must have to overcome translational diffusion. This parameter, $|\omega|^2 t > 6.65 \times 10^3 \ {\rm rad}^2 \ {\rm s}^{-1}$, is also dependent on the time scale (t) for the experiment. In a 100-

second experiment, the helix will overcome diffusion when its frequency is held constant at a minimum of 1.30 Hz. For the same helix, in a 10-second experiment, the helix will overcome diffusion when its frequency is held constant at 4.10 Hz. In an experiment with similar helices and solvent conditions, Patil *et al.*⁵ applied a rotating magnetic field with frequencies in the range 5–15 Hz to propel their microscopic helices, which are well above the predicted minimum threshold frequencies to observe propulsion. Patil *et al.*⁵ also reported that their helices could overcome diffusion when the rotation frequency was 2 Hz.

B. Achiral Swimmers

In Sec. II E, we showed that achiral objects can be divided into two groups by their moments of pitch. The first group consists of achiral objects for which *all* moments of pitch are zero, i.e., the pitch matrix is a null matrix. As a result, objects in this group exhibit no translation-rotation coupling and rotation will not produce displacement. Examples of these achiral non-swimmers are well-known; *e.g.*, spheres, ellipsoids, tetrahedra, and cubes. Interested readers are encouraged to consult Sec. V of the supplementary material for more details.

The second group consists of achiral objects with a special symmetry, where one moment of pitch is zero, while the other two have the same magnitude, but opposite signs. For these objects, the pitch matrix is non-zero and translation-rotation coupling persists. These objects have previously been called *achiral swimmers* because they produce displacements due to rotation. Figure 2 displays an achiral microswimmer: an arrangement of three beads that was experimentally tested by Cheang *et al.* ¹⁷ In their work, Cheang *et al.* reported that a non-vanishing (rt) block of the mobility tensor is required for swimming and, from the symmetry investigations conducted in Ref. 8, concluded that *achiral swimmers* are real.

To triangulate the surface of the three-beads arrangement in Fig. 2, we used the MSMS algorithm³⁶ with a probe radius of $10^{-6} \mu m$ and a triangulation density of 20 vertices/ μm^2 . In Fig. 2, we also found the principal axes of pitch and their associated moments employing the Bead Model developed in Ref. 7 in addition to the boundary element approach developed in this work (Sec. II F). As expected, with both methods of finding the resistance tensor, one moment of pitch is zero and the other two have the same magnitude with a flipped sign.

Utilizing the bead and the boundary element models, Table III presents the translational diffusion and the scalar pitch coefficient for the three-bead achiral swimmer along with the angular

TABLE III. Translational diffusion coefficients and scalar pitch coefficients for the achiral three-beads swimmer in Fig. 2. The translational diffusion coefficients are calculated at 298.15 K with a viscosity of 1.0 mPa·s to mimic the conditions in Ref. 17. Conditions when translation-rotation coupling overtakes translational diffusion are also provided (Eq. (34)).

Hydrodynamic Model	$D_{\rm tt} \left(10^4 \ {\rm nm}^2 \ {\rm s}^{-1}\right)$	$ P /2\pi \left(\text{nm rad}^{-1}\right)$	$ \omega ^2 \times t \left(\text{rad}^2 \text{ s}^{-1} \right)$
Bead (Ref. 7)	6.07	79	> 58
Boundary Element (Sec. II F)	5.80	74	> 64

velocity condition for when the translation-rotation coupling surpasses diffusion. Translational diffusion coefficients were computed at 298.15 K and $\eta = 1.0$ mPa·s, reproducing the experimental conditions of Cheang *et al.*'s work¹⁷ for a NaCl solution. In the first second of an experiment, the translation-rotation coupling of the immersed three-bead swimmer will overtake diffusion when the angular velocity, $|\omega|$, exceeds 7.6 rad s⁻¹ (Bead Model) and 8.0 rad s⁻¹ (Boundary Element Model). These are equivalent to rotational frequencies that exceed 1.3 Hz, and are comparable to the rotating magnetic field frequencies of 1–8 Hz applied by Cheang *et al.*¹⁷ to propel their swimmers. The scalar pitch values in Table III and the moments of pitch in Fig. 2 can be used to generate similar swimming speeds reported in Fig. 3(b) of Ref. 17.

Translational drift is expected when the axes of rotation are not the principal axes of pitch. This translational drift can be seen clearly in the supporting videos¹⁷ displaying the motion of the three-beads swimmers. Hermans *et al.*⁴⁶ also reported translational drift in an experiment with a rotating achiral swimmer. In a Taylor–Couette device, Hermans *et al.*'s achiral swimmer had one orbital radius when rotating clockwise and another when rotating counterclockwise.

C. Lord Kelvin's Isotropic Helicoid

An *isotropic helicoid* is an object for which the blocks of the resistance tensor are isotropic at the center of resistance (CR). That is, the four blocks may be written:⁸

$$\Xi^{tt} = \xi^{tt} \mathbf{I}$$

$$\Xi^{rt}_{CR} = \Xi^{tr}_{CR} = \xi^{tr} \mathbf{I}$$

$$\Xi^{rr}_{CR} = \xi^{rr} \mathbf{I}$$
(35)

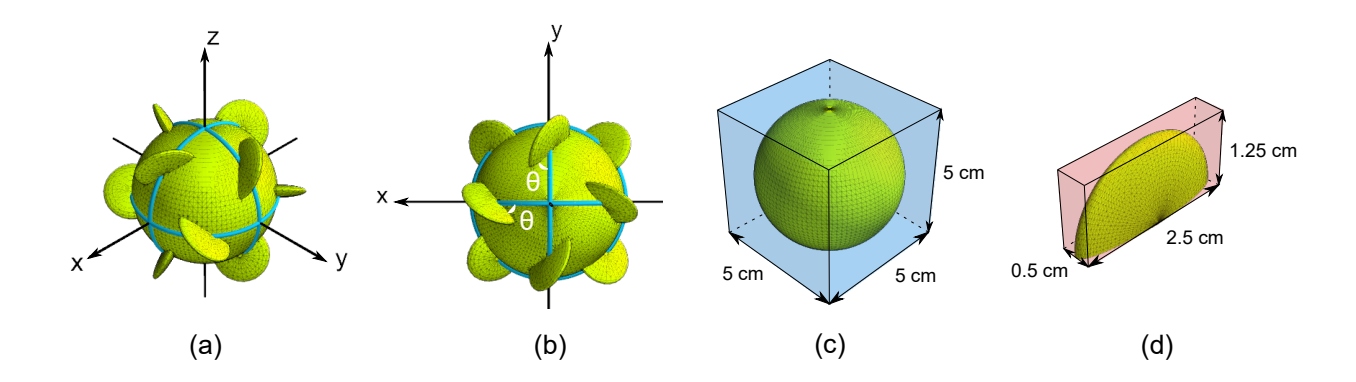


FIG. 5. Generalization of Lord Kelvin's Isotropic Helicoid. (a) Vanes are placed midway between the intersection points of three circles around a sphere. (b) The vanes are tilted at an angle θ relative to the circles, and this angle defines the handedness of the isotropic helicoid. The dimensions of (c) the sphere and (d) the semi-oblate vanes used in our examples.

where ξ^{tt} , ξ^{tr} and ξ^{rr} are scalars and **I** is the 3×3 identity matrix. The only difference between these objects and spherically isotropic bodies (*i.e.*, spheres, cubes and tetrahedra) is that helicoids have non-zero rotation-translation coupling ($\xi^{tr} \neq 0$).

In 1871, Sir William Thomson (widely known as Lord Kelvin) proposed one design for an isotropic helicoid using a sphere with 12 projecting vanes arranged in a systematic way.⁴⁷ A generalization of his approach is shown in Fig. 5 and is described below:^{48,49}

- 1. Center a sphere at the origin, and locate three circles at the intersections of the sphere with the xy-, yz- and xz-planes (Fig. 5(a)).
- 2. Using the six intersection points of the three circles, place the centers of semi-oblate vanes midway between these intersection points. In the end, there will be 4 semi-oblate vanes per circle (Fig. 5(b)).
- 3. The orientation angles θ of the vanes are related to their positions in the circles and defines the handedness of the isotropic helicoid. The isotropic helicoid is right-handed for $0^{\circ} < \theta < 90^{\circ}$ and left-handed for $-90^{\circ} < \theta < 0^{\circ}$. This definition comes from the sign of the angular velocity ω in Eq. (37) and the direction of rotation of a right-handed screw.

We constructed three left-handed isotropic helicoids ($\theta = -30^{\circ}, -45^{\circ}, -60^{\circ}$) and two spherically isotropic bodies ($\theta = 0^{\circ}, -90^{\circ}$) utilizing the procedure in Ref. 48. Each of these isotropic objects are composed of a sphere with 12 semi-oblate vanes whose dimensions are displayed in Fig. 5(c)

and (d). Triangulation of these objects was performed in OpenSCAD,⁵⁰ and we analyzed them employing the boundary element method described in Sec. IIF with a 120-point quadrature developed by Xiao and Gimbutas.⁵¹ This quadrature exactly integrates polynomials of degree 25 and its points and weights are available in Quadpy.²⁶ Figure 6 shows the pitch axes and the moments of pitch for these isotropic objects.

For all five objects in Fig. 6, both the center of resistance and the center of pitch are located at the origin. For the two spherically isotropic bodies, $\Xi_{CR}^{rt} = \Xi_{CR}^{tr} = 0$. From Eq. (8), this implies that the pitch matrix itself is zero and no translation-rotation coupling is possible. The isotropic helicoids ($\theta = -30^{\circ}$, -45° , -60°) have non-zero moments of pitch, but our calculations indicate that these are quite small. From the definition of the pitch matrix, these small moments of pitch are related to small rotation-translation coupling values (ξ^{tr}), and we can use these moments of pitch to demonstrate rotation-translation coupling of isotropic helicoids. For example, in an experiment where an isotropic helicoid from Fig. 6 with $\theta = -45^{\circ}$ is suspended in a viscous fluid and a rotation frequency of 10 Hz is imposed along one of the pitch axes, the helicoid will move 6.3 cm in a 100 s observation time. On the other hand, the spherically isotropic bodies ($\theta = 0^{\circ}$, -90°) will not move at all, since there is no rotation-translation coupling. In the supplementary material (Sec. VI), we compute pitch axes and moments of pitch for a related set of left-handed isotropic helicoids, and we show the pitch coefficients as a function of the vane angle (θ).

Table IV presents the scalar values associated with the blocks of the resistance tensor (Eq. (35)) for the isotropic objects in Fig. 6. These scalar values were computed in silicon oil with $\eta = 490 \text{ mPa} \cdot \text{s}^{52}$ and employing the triangulation and boundary element method described above. For $\theta = -30^{\circ}$, -45° and -60° , the scalar values are related to the isotropic helicoids where $\xi^{\text{tr}} \neq 0$. For $\theta = 0^{\circ}$ and -90° , the scalar values are related to the spherically isotropic bodies where $\xi^{\text{tr}} = 0$.

Rotation-translation coupling can also be demonstrated if we allow an isotropic helicoid or spheroid to fall through a quiescent fluid. The force and torque on the body are:^{8,52}

$$\begin{bmatrix} \mathbf{f} \\ \boldsymbol{\tau} \end{bmatrix} = - \begin{bmatrix} \Xi^{\text{tt}} & \Xi^{\text{rt}}_{\text{CR}} \\ \Xi^{\text{tr}}_{\text{CR}} & \Xi^{\text{rr}}_{\text{CR}} \end{bmatrix} \begin{bmatrix} \mathbf{v} \\ \boldsymbol{\omega} \end{bmatrix} + (m_b - m_f) \begin{bmatrix} \mathbf{g} \\ \mathbf{0} \end{bmatrix} , \qquad (36)$$

where m_b and m_f are the masses of the body and the displaced fluid, respectively, **g** is the gravitational vector field and **0** is the null vector. The term m_b **g** represents the gravitational force and the term $-m_f$ **g**, the force due to buoyancy.

Considering that the body is falling along a single axis, and using the isotropy definitions in

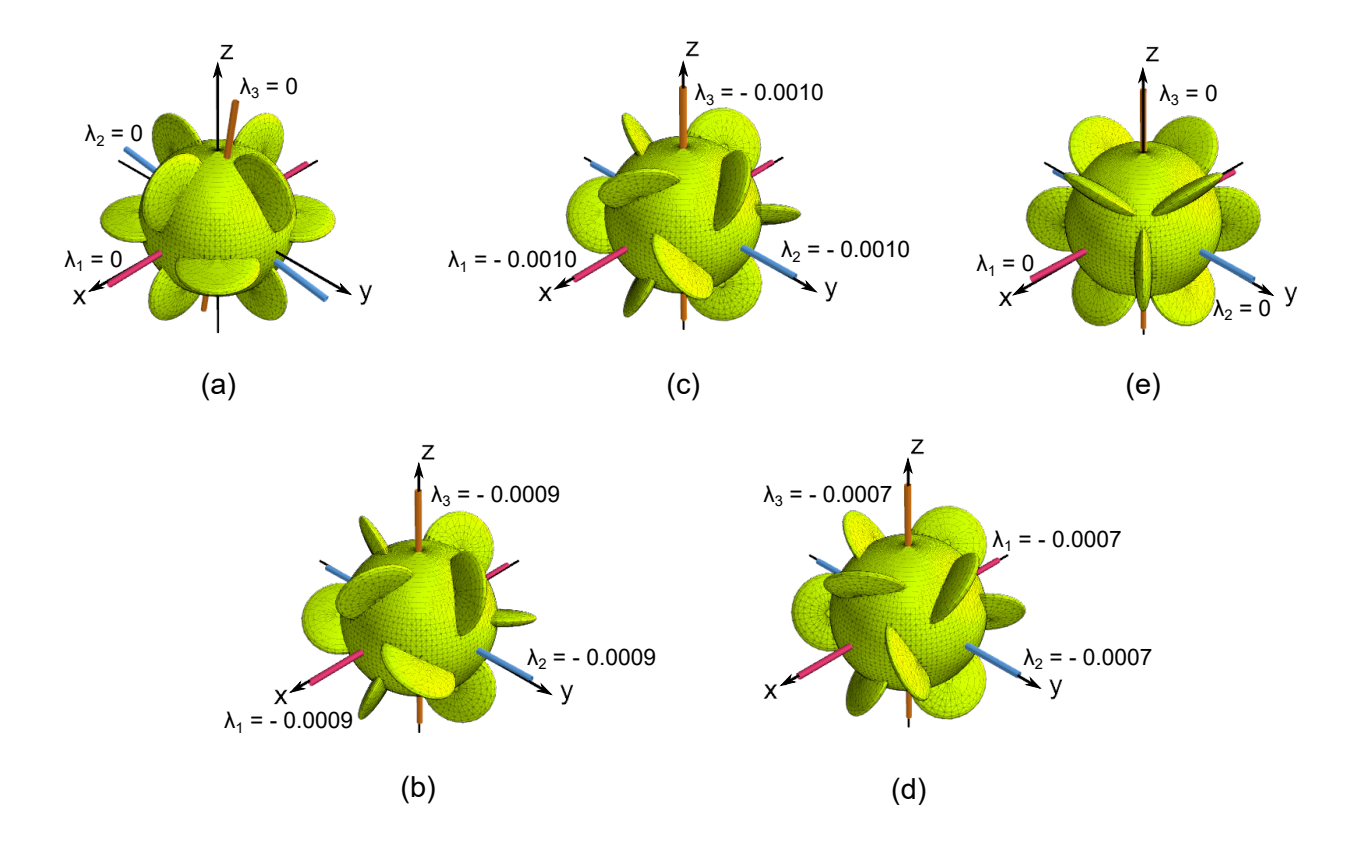


FIG. 6. Moments of pitch (in cm/rad) for isotropic helicoids with different vane angles as described in Fig. 5. When the vanes are at 0° or -90° (panels (a) and (e)), the objects are non-swimmers and do not couple rotation to translation. Pitch axes and moments of pitch indicate that all other vane angles generate non-zero rotation-translation coupling. Here, we show helicoid moments of pitch when the vanes are at -30° , -45° , or -60° (panels (b), (c) and (d)).

Eq. (35), we can compute the terminal velocity and angular velocity,⁸

$$v = \frac{\xi^{rr} (m_b - m_f) g}{\xi^{tt} \xi^{rr} - (\xi^{tr})^2} \quad \text{and} \quad \omega = \frac{-\xi^{tr} (m_b - m_f) g}{\xi^{tt} \xi^{rr} - (\xi^{tr})^2} \quad .$$
 (37)

For chiral objects, we know from our previous work in Ref. 7 that only ξ^{tr} will reverse sign. This implies that v in Eq. (37) is the same for both a helicoid and its mirror image, but the angular velocity ω will flip sign for the mirror image (enantiomeric) version of the object.

For the angular velocity in Eq. (37), Brenner⁸ employed the standard definition of $\omega > 0$ for counterclockwise rotations, following the right-handed rule.¹² This implies $\xi^{tr} < 0$ for right-handed isotropic helicoids, since the scalars ξ^{tt} , ξ^{rr} and $\left[\xi^{tt}\xi^{rr} - \left(\xi^{tr}\right)^2\right]$ are always positive.⁸ We note that this definition is the opposite of the one employed by Gustavsson and Biferale⁴⁹ and Collins *et al.*⁵²

TABLE IV. Scalar parameters for the translational (tt), translation-rotation (tr), and rotational (rr) blocks of the resistance tensor for isotropic helicoids with different vane angles (θ). The moments of pitch for these objects can be obtained from $-\xi^{tr}/\xi^{tt}$. Also shown are the terminal velocities, v, and terminal angular velocities, ω , for these bodies as they fall through a viscous fluid. Using the experimental conditions in Ref. 52, the terminal angular velocities are small, corroborating experimental observations.

Angle	ξ ^{tt}	ζ ^{tr}	ξ ^{rr}	V	ω
	(kg/s)	(kg m/(s rad))	$(kg m^2/(s rad^2))$	(cm/s)	(rad/s)
0°	0.284	0	3.73×10^{-4}	46.8	0
-30°	0.283	2.65×10^{-6}	3.73×10^{-4}	47.0	-3.34×10^{-3}
-45°	0.283	2.72×10^{-6}	3.73×10^{-4}	47.0	-3.42×10^{-3}
-60°	0.283	1.89×10^{-6}	3.73×10^{-4}	47.0	-2.38×10^{-3}
-90°	0.283	0	3.73×10^{-4}	47.0	0

Table IV also provides the terminal velocities and terminal angular velocities for the bodies in Fig. 6. To compute these values, we used $g = 9.81 \text{ m/s}^2$ and the experimental conditions in Ref. 52, *i.e.*, body density $\rho_b = 1.16 \text{ g/cm}^3$ and fluid density $\rho_f = 0.98 \text{ g/cm}^3$ (silicon oil). The mass contributions to the gravitational and buoyant forces can be calculated from the volume of the rigid body, $V_b = 75.267 \text{ cm}^3$, which is the combined volume of the sphere and the 12 semi-oblate vanes in Fig. 5. The spherically isotropic bodies will not manifest angular velocities because their scalar $\xi^{\text{tr}} = 0$. We predict that the left-handed isotropic helicoids will manifest an angular velocity on the order of 10^{-3} rad/s in a clockwise direction.

The scalar friction values, ξ^{tt} , ξ^{tr} and ξ^{rr} scale as ηL , ηL^2 and ηL^3 , respectively, where L is the length of the rigid body. Since the volume V_b scales with L^3 , we conclude that the terminal velocity v and angular velocity v in Eq. (37) will scale as L^2/η and L/η , respectively. To compare with Collins et al.'s helicoid, v we can scale the size of our isotropic helicoid (v = -45°) by 0.348 in the same fluid, and obtain a scaled v = (0.348)v = 5.69 cm/s, and a scaled v = 0.348 v = -1.19×10⁻³ rad/s. Collins v = v = 4.74 cm/s and v = -0.003 rad/s. Since v from Collins v = v = v = 4.74 cm/s and v = -0.003 rad/s. Since v from Collins v = v = v = v = 4.74 cm/s and v = -0.003 rad/s. Since v = v

IV. CONCLUSION

We have presented a general theory for the pitch of objects which are interacting with a fluid medium at low Reynolds number. The pitch matrix, defined in Eq. (5), is diagonalized to yield three pitch axes along with their associated "moments of pitch". The pitch axes and moments arise out of the *geometry* of the objects' surfaces, and they have a number of important properties. First, the symmetry of the object defines the number of degenerate and non-zero moments of pitch. Second, chiral objects (molecules, helices) couple rotational and translational motion in the fluid, and will move in the opposite direction from their enantiomers (mirror images) under the same rotation. Third, the pitch matrix also provides an explanation for the rotation-translation coupling that allows *achiral* swimmers to migrate when they rotate in a fluid. This theory also helps us to understand the translational drift of rotating helical objects. There are many potential uses of this theory, but the primary interest to chemists is to develop an efficient method for separating enantiomers without costly synthetic pathways currently in use.

One of our primary observations is that chiral objects with a C_n axis of symmetry have two degenerate moments of pitch when $n \ge 3$, and there is no drift for rotations around that axis of symmetry. This appears to be the case for propeller-shaped molecules, and this observation points to a general and efficient design principle.

There are many ways to approximate the hydrodynamic resistance tensor, and we have developed a boundary element method which obeys the symmetry properties of the blocks of the resistance tensor. This was also true of earlier methods that use small beads or atomic spheres to represent the surface of an object or the surface of a molecule, but the method for triangulated surfaces given here is generally applicable to rigid bodies of arbitrary shapes.

Our theory of pitch has been tested against some experiments on microswimmers, and our predictions agree well with experimental observations of translational-rotational coupling. We also show results for an object of historical curiosity, Lord Kelvin's isotropic helicoid, which can exhibit a small angular velocity as it falls through a fluid. For the collective behavior of a multi-molecule system, consider Ref. 7, where a competition model was developed to study the separation of chiral molecules in solution. Note that even in racemic mixtures, separation can be achieved under sufficiently large solution vorticities.

There are many potential uses of this theory. Projection of molecular dipoles onto the pitch axis with the largest moment of pitch can help design polarized microwave methods which sep-

arate enantiomers through molecular rotation in the fluid (instead of rotating the fluid around the enantiomers). Additionally, this method also now allows us to identify geometries of achiral swimmers from the eigenvalue structure of the pitch matrix. We also now have a firmer understanding of non-axial drift of chiral objects due to projections of angular velocity onto the axes of pitch.

V. SUPPLEMENTARY MATERIAL

See the supplementary material for additional properties of the pitch matrix and the pitch coefficient, as well as applications of the theory of pitch in isotropic helicoids, achiral swimmers, non-swimmers, and analytically-solvable objects. The supplementary material also develops a relationship between pitch and the moment of inertia for a sphere, and this is used to analyze translation-rotation coupling in spheres rotating in non-Newtonian fluids. An accompanying set of text files provide molecular geometries for the enantiomers and DNA structures, as well as triangulated surfaces for the helix, achiral swimmers, and isotropic helicoids. Code which computes the blocks of the resistance tensor and pitch matrices for these objects is also included.

ACKNOWLEDGMENTS

Support for this project was provided by the National Science Foundation under Grant No. CHE-1954648. Computational time was provided by the Center for Research Computing (CRC) at the University of Notre Dame.

DATA AVAILABILITY STATEMENT

The data that support the findings of this study are available within the article and its supplementary material.

REFERENCES

¹R. S. Ball, *The Theory of Screws: A Study in the Dynamics of a Rigid Body* (Hodges, Foster and Co., Dublin, 1876).

²T. N. Van, T. L. Thanh, and N. Natasa, Manufacturing Technology **21**, 706 (2021).

³N. B. Baranova and B. Y. Zel'dovich, Chem. Phys. Lett. **57**, 435 (1978).

- ⁴D. Schamel, M. Pfeifer, J. G. Gibbs, B. Miksch, A. G. Mark, and P. Fischer, J. Am. Chem. Soc. **135**, 12353 (2013).
- ⁵G. Patil, E. Vashist, H. Kakoty, J. Behera, and A. Ghosh, Appl. Phys. Lett. **119**, 012406 (2021).
- ⁶D. W. Howard, E. N. Lightfoot, and J. O. Hirschfelder, AIChE J. 22, 794 (1976).
- ⁷A. D. S. Duraes and J. D. Gezelter, J. Phys. Chem. B **125**, 11709 (2021).
- ⁸H. Brenner, Chem. Eng. Sci. **19**, 599 (1964).
- ⁹S. Harvey and J. Garcia de la Torre, Macromolecules **13**, 960 (1980).
- ¹⁰H. Brenner, J. Colloid Interface Sci. **23**, 407 (1967).
- ¹¹A. Einstein, "On the Movement of Small Particles Suspended in a Stationary Liquid Demanded by the Molecular-Kinetic Theory of Heat," in *Investigations on the Theory of the Brownian Movement*, edited by R. Fürth (Dover Publications, Inc., Mineola, NY, 1956) pp. 1–18, *translated by* A. D. Cowper.
- ¹²V. B. Bhandari, *Design of Machine Elements*, 3rd ed. (Tata McGraw-Hill Education Private Ltd., New Delhi, 2010) Chap. 6–7, pp. 184–271.
- ¹³R. G. Budynas and J. K. Nisbett, *Shigley's Mechanical Engineering Design*, 9th ed., Mcgraw-Hill Series in Mechanical Engineering (McGraw-Hill, New York, NY, 2011) Chap. 8, pp. 409–473.
- ¹⁴M. L. Ekiel-Jeżewska and E. Wajnryb, J. Phys. Condens. Matter **21**, 204102 (2009).
- ¹⁵K. F. Riley, M. P. Hobson, and S. J. Bence, in *Mathematical Methods for Physics and Engineering* (Cambridge University Press, Cambridge, UK, 2006) Chap. 6, 8, pp. 187–211, 241–315, 3rd ed.
- ¹⁶W. L. Jorgensen, D. S. Maxwell, and J. Tirado-Rives, J. Am. Chem. Soc. **118**, 11225 (1996).
- ¹⁷U. K. Cheang, F. Meshkati, D. Kim, M. J. Kim, and H. C. Fu, Phys. Rev. E **90**, 033007 (2014).
- ¹⁸J. E. Huheey, E. A. Keiter, and R. L. Keiter, "Symmetry and Group Theory," in *Inorganic Chemistry: Principles of Structure and Reactivity* (HarperCollins College Publishers, New York, NY, 1993) Chap. 3, pp. 46–91, 4th ed.
- ¹⁹D. Johnston, "Symmetry@Otterbein," https://symotter.org (accessed January 28, 2023).
- ²⁰R. D. Johnson III, "NIST Computational Chemistry Comparison and Benchmark Database: NIST Standard Reference Database Number 101," (2022), http://cccbdb.nist.gov/ (accessed February 9, 2023).
- ²¹I. Antol, Z. Glasovac, R. Crespo-Otero, and M. Barbatti, J. Chem. Phys. **141**, 074307 (2014).

- ²²J. A. Salthouse and M. J. Ware, *Point Group Character Tables and Related Data* (Cambridge University Press, Cambridge, England, 1972).
- ²³S. A. Allison, Biophys. Chem. **93**, 197 (2001).
- ²⁴S. Kim and S. J. Karrila, *Microhydrodynamics: Principles and Selected Applications*, Butterworth-Heinemann Series in Chemical Engineering (Butterworth-Heinemann, Stoneham, MA, 1991).
- ²⁵G. R. Cowper, Int. J. Numer. Meth. Engng. **7**, 405 (1973).
- ²⁶N. Schlömer, N. Papior, D. Arnold, J. Blechta, and R. Zetter, "Quadpy," version 0.16.10, https://github.com/sigma-py/quadpy (accessed October 3, 2022).
- ²⁷J. García de la Torre and V. A. Bloomfield, Q. Rev. Biophys. **14**, 81 (1981).
- ²⁸B. Carrasco, J. García de la Torre, and P. Zipper, Eur. Biophys. J. **28**, 510 (1999).
- ²⁹B. Carrasco and J. García de la Torre, Biophys. J. **76**, 3044 (1999).
- ³⁰J. García de la Torre and V. Rodes, J. Chem. Phys. **79**, 2454 (1983).
- ³¹A. T. Chwang and T. Y. Wu, Proc. Royal Soc. B **178**, 327 (1971).
- ³²J. J. L. Higdon, J. Fluid Mech. **94**, 331 (1979).
- ³³E. M. Purcell, Proc. Natl. Acad. Sci. U.S.A. **94**, 11307 (1997).
- ³⁴S. Chattopadhyay, R. Moldovan, C. Yeung, and X. L. Wu, Proc. Natl. Acad. Sci. U.S.A. 103, 13712 (2006).
- ³⁵C. Maffeo, L. Quednau, J. Wilson, and A. Aksimentiev, Nat. Nanotechnol. 18, 238 (2023).
- ³⁶M. F. Sanner, A. J. Olson, and J.-C. Spehner, Biopolymers **38**, 305 (1996), *MSMS algorithm*, version 2.6.1; https://ccsb.scripps.edu/msms/ (accessed November 5, 2022).
- ³⁷O. Bottema and B. Roth, "Two Positions Theory," in *Theoretical Kinematics* (Dover Publications, Inc., Mineola, NY, 1990) Chap. 3, pp. 35–62.
- ³⁸H. Ceylan, I. C. Yasa, O. Yasa, A. F. Tabak, J. Giltinan, and M. Sitti, ACS Nano **13**, 3353 (2019).
- ³⁹J. S. Hardwick, D. Ptchelkine, A. H. El-Sagheer, I. Tear, D. Singleton, S. E. V. Phillips, A. N. Lane, and T. Brown, Nat. Struct. Mol. Biol. 24, 544 (2017).
- ⁴⁰L. Lercher, M. A. McDonough, A. H. El-Sagheer, A. Thalhammer, S. Kriaucionis, T. Brown, and C. J. Schofield, Chem. Commun. **50**, 1794 (2014).
- ⁴¹Z. Luo, M. Dauter, and Z. Dauter, Acta Crystallogr. D **70**, 1790 (2014).
- ⁴²A. Ben-Naim, "Application of Statistical Mechanics in the Study of Liquid Water," in *Water,* a *Comprehensive Treatise: The Physics and Physical Chemistry of Water*, Vol. 1, edited by

- F. Franks (Plenum Press, New York, NY, 1972) Chap. 11, pp. 413–442.
- ⁴³W. Saenger, "Polymorphism of DNA versus Structural Conservatism of RNA: Classification of A-, B-, and Z-Type Double Helices," in *Principles of Nucleic Acid Structure*, Springer Advanced Texts In Chemistry, edited by C. R. Cantor (Springer-Verlag, New York, NY, 1984) Chap. 9, pp. 220–241.
- ⁴⁴S. McNicholas, E. Potterton, K. S. Wilson, and M. E. M. Noble, Acta Crystallogr. D **67**, 386 (2011), *CCP4mg*, version 2.10.11; https://www.ccp4.ac.uk/MG/ (accessed November 5, 2022).
- ⁴⁵CRC Handbook, "Section 6: Fluid Properties," in *CRC Handbook of Chemistry and Physics*, edited by J. R. Rumble (CRC Press/Taylor & Francis, Boca Raton, FL, 2022) 103rd ed., Online version 2022.
- ⁴⁶T. M. Hermans, K. J. M. Bishop, P. S. Stewart, S. H. Davis, and B. A. Grzybowski, Nat. Commun. **6**, 5640 (2015).
- ⁴⁷W. Thomson, London, Edinburgh Dublin Philos. Mag. J. Sci. **42**, 362 (1871).
- ⁴⁸C. Frost, "Isotropic-Helicoid: Lord Kelvin's Hypothesized Shape," (2021), https://github.com/chadfrost/isotropic-helicoid (accessed November 8, 2022).
- ⁴⁹K. Gustavsson and L. Biferale, Phys. Rev. Fluids 1, 054201 (2016).
- ⁵⁰"OpenSCAD," (2021), version 2021.01; https://openscad.org/ (accessed November 21, 2022).
- ⁵¹H. Xiao and Z. Gimbutas, Comput. Math. Appl. **59**, 663 (2010).
- ⁵²D. Collins, R. J. Hamati, F. Candelier, K. Gustavsson, B. Mehlig, and G. A. Voth, Phys. Rev. Fluids **6**, 074302 (2021).